Electronic Supplementary Material (ESI) for RSC Advances.

Supplementary materials

1 Materials and Methods

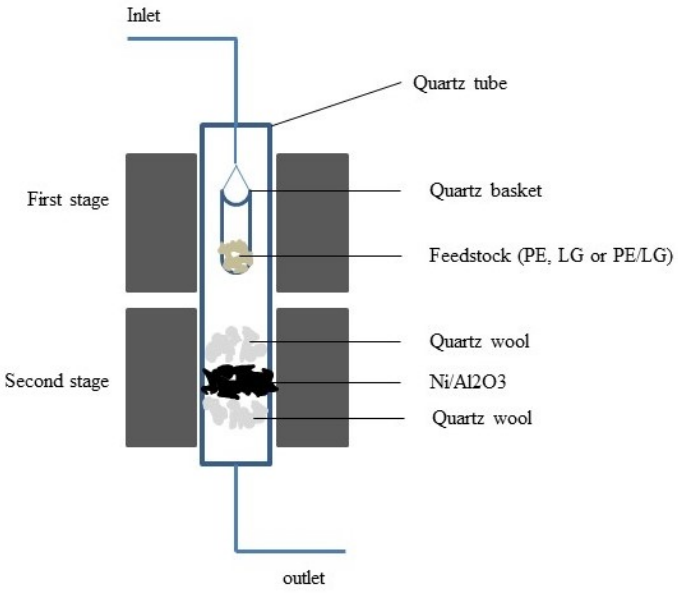

Fig. S1 Setup employed in present study

2 Results and discussion

2.1 Characteristics of fresh NiO/Al_2O_3 catalyst

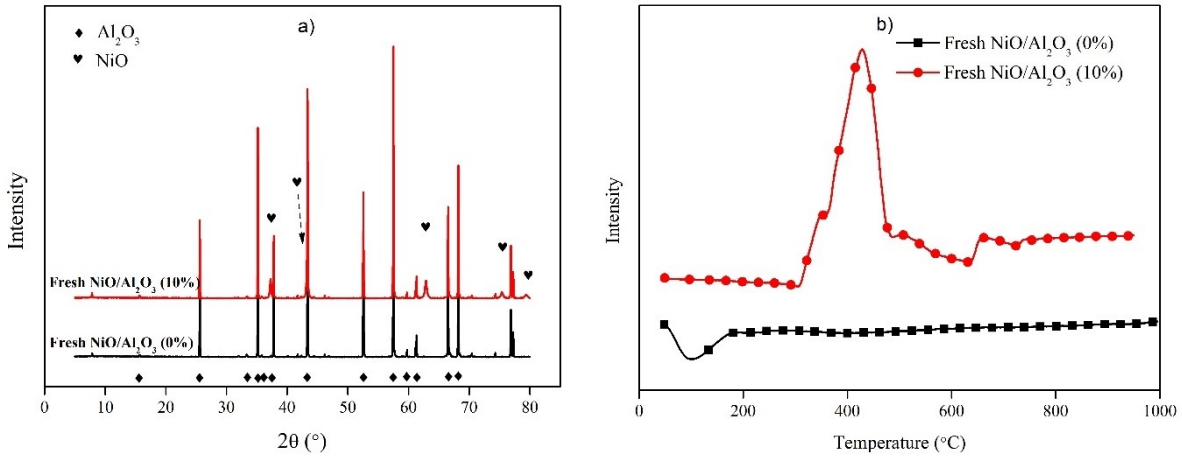

Fig. S2 XRD patterns (a) and H_2-TPR curves (b) of fresh NiO/Al_2O_3 with 0% and 10% Ni content

Fig. S2a shows the XRD results of the home-made fresh NiO/Al_2O_3 with different Ni content (0%-10%). Two types of substances, NiO (spade) and Al_2O_3 (diamond) can be found according to the diffraction peaks. Particularly, PDF card (JCPDS 78-0643) reveals that the characteristic peaks of NiO species mainly occur at 2Θ = 37.3°, 43.4°, 63.0°, 75.6° and 79.6°, which are index to (1 1 1), (2 0 0), (2 2 0), (3 1 1) and (3 2 2) NiO [1]. Ni content in fresh NiO/Al_2O_3 is further detected by AAS and the result is presented in **Table S1**. It can be seen that Ni content (m_{Ni}/m_{Al2O3}) of fresh NiO/Al_2O_3 (0%) and fresh NiO/Al_2O_3 (10%) are 0 and 100.38 mg/g, respectively. This indicates that the real Ni content in fresh NiO/Al_2O_3 (0%) and fresh NiO/Al_2O_3 (10%) are 0% and 10.04%, respectively, which is highly closed to theoretical ones (i.e., 0% and 10%).

Table S1 Ni content in fresh NiO/Al_2O_3 catalysts detected by AAS

	Ni content[a]		Ni content[b]	
	mg/g	%	mg/g	%
Fresh NiO/Al_2O_3 (0%)	0	0	0	0
Fresh NiO/Al_2O_3 (10%)	89.01	8.90	100.38	10.04

a is the ratio of m_{Ni} to $m_{(NiO+Al2O3),}$ bis the ratio of m_{Ni} to m_{Al2O3}

The H_2-TPR curves of fresh NiO/Al_2O_3 with different Ni content (0%-10%) are showed in **Fig. S2b** to clarify the interaction between NiO and substrate (i.e., Al_2O_3). Reduction peak related to NiO can not be found in fresh NiO/Al_2O_3 (0%) due to it contains no Ni content. Whereas fresh NiO/Al_2O_3 (10%) exhibits several broad and asymmetric H_2 consumption peaks, which can attribute to the reduction of NiO possessing varying strength of interaction-bonding with Al_2O_3. In detail, the pronounced H_2 consumption peak centered at 428 ℃ assigns to the reduction of NiO species, which have a weak interaction with Al_2O_3. By comparison, two relatively weak H_2 consumption peaks occurred at 508 and 660 ℃ correspond to the reduction of the Ni^{2+} ions in strong octahedral and tetrahedral coordination with Al_2O_3, respectively [2]. It is reported that peaks at 400-500, 500-600 and > 600 ℃ can be assigned to weak, medium and strong interaction between NiO and Al_2O_3, respectively [3]. A weak interaction between active component and substrate would result in the migration and aggregation of active component when the catalyst is employed in a catalytic reforming process. While the catalyst possesses a relatively stable structure when the active component and substrate exhibit a medium or strong

interaction.

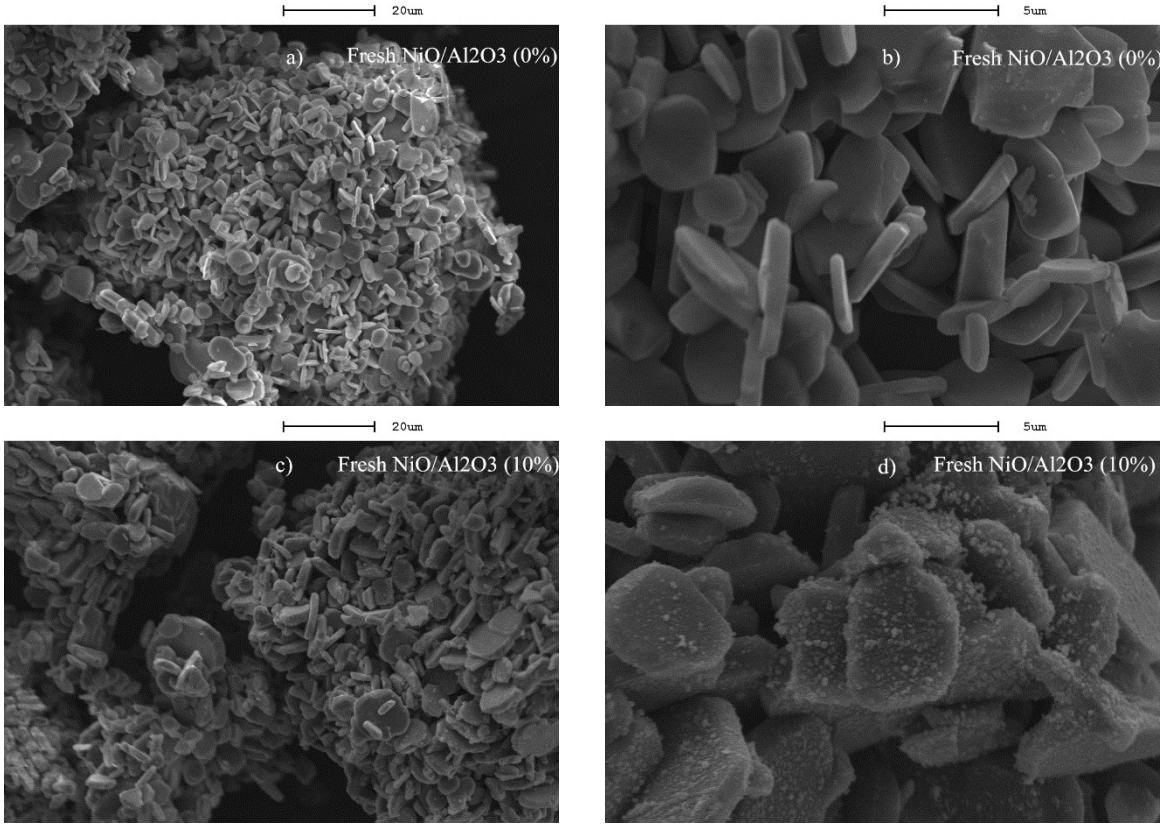

Fig. 2 SEM images of fresh NiO/Al_2O_3 with different Ni content, (a-b) 0%, (c-b) 10%

The morphological features of fresh NiO/Al_2O_3 with different Ni content (0%-10%) characterized using SEM are presented in **Fig. S3**. It can be found that Al_2O_3 employed as substrate in NiO/Al_2O_3 catalyst shows a round cake-like structure with a diameter in the range of 2-6 μm and a thickness ranging from 0.5 to 1.2 μm (**Fig. S3 a-b**). After the treatment of Ni (fresh NiO/Al_2O_3 (10%)), a large amount of nano NiO particles with a diameter in the range of 40-120 nm uniformly dispersed over the surface of Al_2O_3 can be observed in **Fig. S3 c-d**. Good dispersion and uniform particle size of NiO would provide fresh NiO/Al_2O_3 (10%) a superior catalytic capability. The textural properties of fresh NiO/Al_2O_3 with different Ni content (0%-

10%) is shown in **Table S2**. The specific surface area (SSA), total pore volume (TPV) and average pore diameter (APD) of fresh NiO/Al_2O_3 (0%) are 23.29 m^2/g, 0.07 cm^3/g and 13.24, respectively. According to the SEM results as shown in **Fig. S3**, the pore structure of fresh NiO/Al_2O_3 (0%) may be originated from the randomly stacking of the round cake-like Al_2O_3. The introduction of nano NiO particles via an impregnation process in combination with a calcination process causes the evident decrease of SSA and TPV due to the presence of nano NiO particles that might block the porous structure.

Table S2 Pore characteristics of fresh Ni/Al_2O_3 catalysts with different Ni content

	SSA[a] (m^2/g)	MP SSA[b] (m^2/g)	TPV[c] (cm^3/g)	MPV[d] (cm^3/g)	APD[e] (nm)
Fresh NiO/Al_2O_3 (0%)	23.29	4.07	0.07	0.002	13.24
Fresh NiO/Al_2O_3 (10%)	1.71	1.32	0.01	0.0006	18.68

a is specific surface area; b is micropore specific surface area, c is totap pore volume; d is micropore pore volune; e is average pore diameter.

Table S3 Comparison of the maximum capacity of Pb(II) adsorption by CNTs-related adsorbents

Adsorbents	Adsorption capacity (mg/g)	Conditions	References
Pristine materials			
Acetylene-derived CNTs	2.05	pH 6.0, at 20 ℃, 48 h	[4]
Propylene-derived CNTs	17.44	pH 5.0, at room temperature, 6 h	[5]
Commercial CNTs	2.94	pH 6.2, at 25 ℃, 200 min	[6]
Acetylene-derived CNTs	17.54	pH 6.0, at 20 ℃, 24 h	[7]
γ-Al_2O_3	12.64	pH 3.0, at 25 ℃	[8]
Al_2O_3	22.4	pH 4.0, at 25 ℃, 24 h	[9]
Composites			
CNTs/bagasse composite	56.6	pH 4.5, at 28 ℃, 24 h	[10]
Oxidized CNTs-CI_2 composite	87.57	pH 5.0, at 45 ℃, 2 h	[11]
CNTs/$CoFe_2O_4$ composite	140.4	pH 6.0, at 30 ℃, 12 h	[12]
CNTs@SiO_2-NH_2 composite	147.1	pH 5.2, at 45 ℃, 24 h	[13]
CNTs@zeolite composite	55.74	pH 5.0, at 40 ℃, 12 h	[14]
Organo-functionalized SiO_2-Al_2O_3	92.0	pH 6.5, at 25 ℃, 2 h	[15]
2,4-dinitrophenylhydrazine-modified γ-Al_2O_3	100.00	pH 5.0, at 25 ℃, 1.5 h	[16]
Al_2O_3-supported iron oxide	29.01	pH 5.0, at 45 ℃, 48 h	[17]
PE/LG-CNTs-Ni/Al_2O_3 composites	146.077	pH 5.0, at 25 ℃, 8 h	Present study

References:

[1] Z. Zhang, X. Hu, L. Zhang, Y. Yang, Q. Li, H. Fan, Q. Liu, T. Wei, C.-Z. Li, Steam reforming of guaiacol over Ni/Al2O3 and Ni/SBA-15: Impacts of support on catalytic behaviors of nickel and properties of coke, Fuel Processing Technology, 191 (2019) 138-151.

[2] V. Claude, J.G. Mahy, J. Geens, S.D. Lambert, Ni-doped γ-Al2O3 as secondary catalyst for bio-syngas purification: influence of Ni loading, catalyst preparation, and gas composition on catalytic activity, Materials Today Chemistry, 13 (2019) 98-109.

[3] Y. Xu, X.-h. Du, J. Li, P. Wang, J. Zhu, F.-j. Ge, J. Zhou, M. Song, W.-y. Zhu, A comparison of Al2O3 and SiO2 supported Ni-based catalysts in their performance for the dry reforming of methane, Journal of Fuel Chemistry and Technology, 47 (2019) 199-208.

[4] D. Xu, X. Tan, C. Chen, X. Wang, Removal of Pb(II) from aqueous solution by oxidized multiwalled carbon nanotubes, Journal of Hazardous Materials, 154 (2008) 407-416.

[5] Y.-H. Li, S. Wang, J. Wei, X. Zhang, C. Xu, Z. Luan, D. Wu, B. Wei, Lead adsorption on carbon nanotubes, Chemical Physics Letters, 357 (2002) 263-266.

[6] G.D. Vuković, A.D. Marinković, S.D. Škapin, M.Đ. Ristić, R. Aleksić, A.A. Perić-Grujić, P.S. Uskoković, Removal of lead from water by amino modified multi-walled carbon nanotubes, Chemical Engineering Journal, 173 (2011) 855-865.

[7] X. Ren, D. Shao, S. Yang, J. Hu, G. Sheng, X. Tan, X. Wang, Comparative study of Pb(II) sorption on XC-72 carbon and multi-walled carbon nanotubes from aqueous

solutions, Chemical Engineering Journal, 170 (2011) 170-177.

[8] Y.J.O. Asencios, M.R. Sun-Kou, Synthesis of high-surface-area γ-Al2O3 from aluminum scrap and its use for the adsorption of metals: Pb(II), Cd(II) and Zn(II), Applied Surface Science, 258 (2012) 10002-10011.

[9] H. Zhang, L. Gu, L. Zhang, S. Zheng, H. Wan, J. Sun, D. Zhu, Z. Xu, Removal of aqueous Pb(II) by adsorption on Al2O3-pillared layered MnO2, Applied Surface Science, 406 (2017) 330-338.

[10] I.A.A. Hamza, B.S. Martincigh, J.C. Ngila, V.O. Nyamori, Adsorption studies of aqueous Pb(II) onto a sugarcane bagasse/multi-walled carbon nanotube composite, Physics and Chemistry of the Earth, Parts A/B/C, 66 (2013) 157-166.

[11] J.-Y. Yang, X.-Y. Jiang, F.-P. Jiao, J.-G. Yu, X.-Q. Chen, Fabrication of diiodocarbene functionalized oxidized multi-walled carbon nanotube and its aqueous adsorption performance toward Pb(II), Environmental Earth Sciences, 76 (2017).

[12] L. Zhou, L. Ji, P.-C. Ma, Y. Shao, H. Zhang, W. Gao, Y. Li, Development of carbon nanotubes/CoFe2O4 magnetic hybrid material for removal of tetrabromobisphenol A and Pb(II), Journal of Hazardous Materials, 265 (2014) 104-114.

[13] K. Yang, Z. Lou, R. Fu, J. Zhou, J. Xu, S.A. Baig, X. Xu, Multiwalled carbon nanotubes incorporated with or without amino groups for aqueous Pb(II) removal: Comparison and mechanism study, Journal of Molecular Liquids, 260 (2018) 149-158.

[14] D.K. Venkata Ramana, D.H. Kumar Reddy, B.N. Kumar, K. Seshaiah, G.P. Chandra Rao, C. Lu, Adsorption of Pb(II) from Aqueous Solutions by Chemically

Modified Zeolite supported Carbon Nanotubes: Equilibrium, Kinetic, and Thermodynamic Studies, Separation Science and Technology, 48 (2013) 403-412.

[15] M. Boroumand Jazi, M. Arshadi, M.J. Amiri, A. Gil, Kinetic and thermodynamic investigations of Pb(II) and Cd(II) adsorption on nanoscale organo-functionalized SiO2Al2O3, Journal of Colloid and Interface Science, 422 (2014) 16-24.

[16] A. Afkhami, M. Saber-Tehrani, H. Bagheri, Simultaneous removal of heavy-metal ions in wastewater samples using nano-alumina modified with 2,4-dinitrophenylhydrazine, Journal of Hazardous Materials, 181 (2010) 836-844.

[17] Y.-H. Huang, C.-L. Hsueh, C.-P. Huang, L.-C. Su, C.-Y. Chen, Adsorption thermodynamic and kinetic studies of Pb(II) removal from water onto a versatile Al2O3-supported iron oxide, Separation and Purification Technology, 55 (2007) 23-29.